

MOL # 117499

**Metal coordination is crucial for GGPPS-bisphosphonates interactions: A  
crystallographic and computational analysis**

Michal Lisnyansky, Elon Yariv, Omri Segal, Milit Marom, Anat Loewenstein, Nir Ben-Tal,  
Moshe Giladi, Yoni Haitin

Department of Physiology and Pharmacology, Sackler Faculty of Medicine, Tel Aviv  
University, Tel Aviv, Israel (ML, MM, MG, YH)

Department of Biochemistry and Molecular Biology, George S. Wise Faculty of Life  
Sciences, Tel Aviv University, Tel Aviv, Israel (EY, NB-T)

Sackler Faculty of Medicine, Tel Aviv University, Tel Aviv, Israel (OS, AL)

Ophthalmology Division, Tel Aviv Sourasky Medical Center, Tel Aviv, Israel (AL)

Tel Aviv Sourasky Medical Center, Tel Aviv, Israel (MG)

MOL # 117499

**Running title: Metal-bisphosphonates interactions in GGPPS**

**Corresponding authors:**

**Dr. Moshe Giladi and Dr. Yoni Haitin**

Department of Physiology and Pharmacology

Sackler Faculty of Medicine

Tel Aviv University, Tel Aviv, Israel

email: [moshegil@post.tau.ac.il](mailto:moshegil@post.tau.ac.il) (M.G.), [yhaitin@post.tau.ac.il](mailto:yhaitin@post.tau.ac.il) (Y.H.)

Phone: +972-3-6409261 Fax: +972-3-6409113

Text pages: 31

Number of tables: 5 + 1 supplemental

Number of figures: 5 + 4 supplemental

Number of references: 57

Number of words in the *Abstract*: 190

Number of words in the *Introduction*: 750

Number of words in the *Discussion*: 1162

**Abbreviations:**

CN, coordination number; CSD, Cambridge Structural Database; DSF, differential scanning fluorimetry; FPP, farnesyl diphosphate; FPPS, farnesyl diphosphate synthase; GGPP, geranylgeranyl diphosphate; GGPPS, geranylgeranyl diphosphate synthase; HEPES, 4-(2-hydroxyethyl)-1-piperazineethanesulfonic acid; IPP, isopentenyl diphosphate; MBP, metal binding pharmacophore; IPTG, isopropyl  $\beta$ -D-1-thiogalactopyranoside; mmGBSA, molecular mechanic combined with the generalized born and surface continuum solvation; NTA, Nitrilotriacetic acid; PMSF, phenylmethane sulfonyl fluoride; TCEP, tris(2-carboxyethyl)phosphine;  $T_m$ , melting temperature; TSA, thermal shift assay.

MOL # 117499

## Abstract

Geranylgeranyl diphosphate synthase (GGPPS) is a central metalloenzyme in the mevalonate pathway, crucial for the prenylation of small GTPases. As small GTPases are pivotal for cellular survival, GGPPS was highlighted as a potential target for treating human diseases, including solid and hematological malignancies and parasitic infections. Most available GGPPS inhibitors are bisphosphonates, but the clinically available compounds demonstrate poor pharmacokinetic properties. Although the design of novel bisphosphonates with improved physicochemical properties is highly desirable, the structure of wild-type human GGPPS (hGGPPS) bound to a bisphosphonate has not been resolved. Moreover, various metal-bisphosphonate binding stoichiometries were previously reported in structures of yeast GGPPS (yGGPPS), hampering computational drug design with metal binding pharmacophores (MBP). Here, we report the 2.2 Å crystal structure of hGGPPS in complex with ibandronate, clearly depicting the involvement of three  $Mg^{2+}$  ions in bisphosphonate-protein interactions. Using drug binding assays and computational docking, we show that the assignment of three  $Mg^{2+}$  ions to the binding site of both hGGPPS and yGGPPS greatly improves the correlation between calculated binding energies and experimentally measured affinities. This work provides a structural basis for future rational design of additional MBP-harboring drugs targeting hGGPPS.

MOL # 117499

### **Significance statement**

Bisphosphonates are inhibitors of GGPPS, a metalloenzyme crucial for cell survival. Bisphosphonates binding depends on coordination by  $Mg^{2+}$  ions, but various  $Mg^{2+}$ -bisphosphonate binding stoichiometries were previously reported. Here, we show that three  $Mg^{2+}$  ions are vital for drug binding and provide a structural basis for future computational design of GGPPS inhibitors.

MOL # 117499

## Introduction

Geranylgeranyl diphosphate (GGPP, C<sub>20</sub>) synthase (GGPPS) is an important mevalonate pathway *trans*-prenyltransferase (Liang *et al.*, 2002). By catalyzing the condensation of isopentenyl pyrophosphate (IPP, C<sub>5</sub>) with farnesyl diphosphate (FPP, C<sub>15</sub>), GGPPS synthesizes GGPP, used for post-translational protein prenylation (Wang and Casey, 2016) (Figure 1). Intriguingly, while the fungal, bacterial and plant orthologs exhibit dimeric structures, human GGPPS (hGGPPS) forms a hexamer composed of three dimers (Kavanagh *et al.*, 2006a).

Protein prenylation is crucial for the membrane association and function of proteins essential for cellular survival. Importantly, most small GTPases, including pivotal oncogenes such as RAS and RHO, require prenylation for their normal function (Bourne *et al.*, 1990; Konstantinopoulos *et al.*, 2007), making inhibition of this process an attractive therapeutic target. Indeed, bisphosphonates are a group of drugs that induce cellular apoptosis by inhibiting isoprenoid biosynthesis (Kavanagh *et al.*, 2006b). Currently, bisphosphonates are used to treat osteoporosis, a common skeletal disorder (Russell, 2011). By specifically incorporating into the bone matrix, the drug is released upon resorption by osteoclasts, undergoes endocytosis and inhibits GGPPS, along with the upstream enzyme FPP synthase (FPPS) (Guo *et al.*, 2007; Russell, 2011). The resultant decrease in small GTPases prenylation leads to osteoclasts apoptosis and decreased bone resorption (Russell, 2011).

The profound cellular alterations induced by inhibition of protein prenylation, and specifically, by a decrease in prenylation of small GTPases (Russell, 2011), highlighted GGPPS as a potential target for cancer therapy (Downward, 2003; Jiang *et al.*, 2014; Mullen *et al.*, 2016; Lacbay *et al.*, 2018). Moreover, GGPPS enzymes from parasites leading to human diseases are considered as potential drug targets to inhibit parasitic growth *in vitro* and *in vivo* (Szabo *et al.*, 2002; Ricci *et al.*, 2016). However, the physicochemical properties of the marketed bisphosphonates render them with poor bioavailability and cell permeability characteristics (Lin, 1996), restricting their therapeutic scope for treatment of bone disorders, where the drug accumulates locally and permeates the cell membrane *via* endocytosis during

MOL # 117499

bone resorption (Russell, 2011). Thus, to exploit the full potential of GGPPS inhibition, the design of novel bisphosphonates with modified pharmacokinetic characteristics is required for expansion of their target tissues repertoire (Haney *et al.*, 2017).

Over the past two decades, several attempts were made to establish robust computational screening approaches to predict the binding potency of bisphosphonates to GGPPS (Szabo *et al.*, 2002; Guo *et al.*, 2007; Haney *et al.*, 2017). These attempts were based on the wealth of structural information obtained using the yeast GGPPS (yGGPPS) ortholog bound to various bisphosphonates (Guo *et al.*, 2007; Hudock *et al.*, 2008; Zhang *et al.*, 2009), despite differences in the potency of these drugs towards yGGPPS and hGGPPS (Guo *et al.*, 2007), as the structure of hGGPPS-WT bound to a bisphosphonate was unavailable.

We have recently determined the crystal structure of hGGPPS-D188Y, involved in bisphosphonates-induced atypical fractures, in complex with zoledronate (Lisnyansky *et al.*, 2018). Our analysis revealed the involvement of three Mg<sup>2+</sup> ions in GGPPS-bisphosphonate interaction, a metal-ligand stoichiometry deviating from that observed in most previously determined yeast GGPPS structures (Lisnyansky *et al.*, 2018). Bisphosphonates harbor a metal binding pharmacophore (MBP) that allows strong protein-ligand interactions mediated by coordinated metal ions (Cohen, 2017; Jiang *et al.*, 2019). However, the use of such MBPs in drug design requires accurate positioning of metal ions in the binding site (Harding *et al.*, 2010; Harding *et al.*, 2018). Importantly, the assignment of Mg<sup>2+</sup> ions, involved in GGPPS-bisphosphonates interactions, has proven to be especially challenging (Nayal and Di Cera, 1996; Zheng *et al.*, 2008).

The discrepancy in the metal-ligand interaction network observed in the mutant hGGPPS, compared with previously determined yGGPPS structures, yield profound ramifications on computational drug screening and design attempts due to the different electrostatic and steric properties of the binding pocket. Indeed, exploration of the chemical space in the design of metalloenzyme inhibitors greatly depends on metal-ligand interactions (Riccardi *et al.*, 2018). Moreover, molecular docking taking into account metal-ligand interactions have proven successful in obtaining potent and specific metalloenzymes inhibitors

MOL # 117499

(Bruno *et al.*, 2017). Therefore, we have determined the first crystal structure of hGGPPS-WT in complex with the bisphosphonate ibandronate. Furthermore, to explore possible ortholog-dependent structural differences in metal-ligand coordination, we have reanalyzed eight previously solved structures of  $\gamma$ GGPPS in complex with various bisphosphonates and assigned previously misidentified  $Mg^{2+}$  ions to the bisphosphonates binding site. Using a conjunction of drug binding assays and computational docking, we show the essential role of  $Mg^{2+}$  ions stoichiometry in GGPPS-bisphosphonates interaction and the contribution of metal-ligand interactions to the predictivity of computational models for GGPPS inhibitors.

MOL # 117499

## Materials and Methods

**Overexpression and purification of hGGPPS** – cDNA of full-length human *GGPS1* (transOMIC, Huntsville, AL, USA) was cloned into pETM-11 vector with N-terminal hexahistidine tag followed by a TEV protease cleavage site. Proteins were overexpressed and purified as previously described (Kavanagh *et al.*, 2006a; Lisnyansky *et al.*, 2018), using immobilized metal affinity chromatography and size-exclusion chromatography. Briefly, *E. coli* T7 express competent cells, transformed with the GGPPS construct, were grown in Terrific Broth medium at 37°C until reaching  $OD_{600nm} = 0.6$  and induced at 16°C by adding 0.5 mM isopropyl  $\beta$ -D-1-thiogalactopyranoside (IPTG). Proteins were expressed at 16°C for 16-20 h and harvested by centrifugation (10,000xg for 10 min). Cells were suspended in buffer A, containing 50 mM HEPES, pH 7.5, 500 mM NaCl, 5% glycerol, 0.5 mM tris(2-carboxyethyl)phosphine (TCEP), 1  $\mu$ g/ml DNase I, 1 mM phenylmethane sulfonyl fluoride (PMSF) and Protease Inhibitor Cocktail Set III (Calbiochem, San Diego, CA, USA). The cells were disrupted in an EmulsiFlex C3 homogenizer (Avestin Inc., Ottawa, ON, Canada). The soluble protein was then recovered by centrifugation at  $\sim 32,000xg$  for 45 min at 4 °C. The supernatant was loaded onto a  $Ni^{2+}$ -NTA column, followed by thorough washing with buffer A, supplemented with 30 mM imidazole to reduce nonspecific protein binding. Next, overexpressed proteins were eluted with buffer A supplemented with 250 mM imidazole. Imidazole was removed using a HiPrep 26/10 desalting column equilibrated with buffer A, followed by the addition of 6xHis-tagged TEV protease (1 mg TEV protease per 50 mg protein) to the eluate, to remove their 6xHis-tagged, at 4°C overnight. The cleaved proteins were then loaded again onto a  $Ni^{2+}$ -NTA column pre-equilibrated with buffer A containing 30 mM imidazole to remove the cleaved 6xHis-tag and TEV protease. The flow-through was collected, concentrated to 3-4 mL, and loaded onto a HiLoad 16/60 superdex-200 column (GE healthcare, UK) equilibrated with 10 mM HEPES, pH 7.5, 100 mM NaCl, 1mM  $MgCl_2$ , 0.5 mM TCEP for final purification. Purified proteins were concentrated and flash-frozen in liquid nitrogen and stored at -80°C.

MOL # 117499

**Crystallization and structure determination of ibandronate-bound hGGPPS** – Initial crystallization screens were performed using 38 mg/mL purified hGGPPS at 19°C using the sitting drop vapor diffusion method. Initial crystals were obtained in 0.1 M sodium formate, pH 7.0, 12% w/v PEG 3350. Crystals were soaked overnight with mother liquor solution supplemented with 350  $\mu$ M ibandronate, cryoprotected with 20% glycerol and immersed in liquid N<sub>2</sub>. Data were collected at 100°K at the European Synchrotron Radiation Facility (ESRF; Grenoble, France). Integration, scaling and merging of the diffraction data were done with the XDS program (Kabsch, 2010). As the data were slightly anisotropic, an ellipsoidal truncation and anisotropic scaling were performed (Strong *et al.*, 2006) using resolution cutoffs of  $a^* = 2.3 \text{ \AA}$ ,  $b^* = 2.2 \text{ \AA}$ ,  $c^* = 2.2 \text{ \AA}$ . The structure was solved by molecular replacement using the programs PHASER (McCoy *et al.*, 2007) and PHENIX (Adams *et al.*, 2010) (Table 1). The structure of a single dimer from GGPPS-WT (PDB 2Q80) was used as a search model. Iterative model building and refinement were carried out in PHENIX with manual adjustments using COOT (Emsley and Cowtan, 2004). Structural illustrations were prepared with UCSF Chimera (<https://www.cgl.ucsf.edu/chimera>) or PyMOL (<https://pymol.org>). Atomic coordinates and structure factors for the structure of hGGPPS in complex with ibandronate have been deposited in the Protein Data Bank with accession number 6R4V.

**Assignment of Mg<sup>2+</sup> ions** – To assign Mg<sup>2+</sup> ions, we have used several restraints including the average bond lengths, CN and the identity of the oxygen donors (Table 4). The usual CN for Mg<sup>2+</sup> in proteins is 6, with 1-2 protein donor oxygen atoms and the rest arising from phosphate groups and water molecules. However, incomplete coordination spheres in medium resolution structures (2-2.5  $\text{\AA}$ ), as the available structures of yGGPPS, are commonly observed. Therefore, we used the average coordination number ( $4.5 \pm 1.5$ ) in medium-resolution structures (Zheng *et al.*, 2008) and considered binding sites with CN = 3-6. In addition, although based on the CSD (Kennard, 2015) the average Mg<sup>2+</sup>-O bond length is 2.16  $\text{\AA}$ , in the given resolution range and using a cutoff of 3  $\text{\AA}$  to define the coordination sphere, the mean Mg<sup>2+</sup>-O bond length is  $2.24 \pm 0.26 \text{ \AA}$  with a complete coordination sphere (CN  $\geq 5$ )

MOL # 117499

and  $2.37 \pm 0.32$  Å with an incomplete coordination sphere (CN < 5) (Zheng *et al.*, 2008). These bond length values were used as reference in the current analysis.

**Differential scanning fluorimetry (DSF)** – Thermal shift assay (TSA) was performed using a real-time PCR system (Thermo Fisher Scientific, Waltham, MA, USA) with the fluorescent dye SYPRO Orange (Thermo Fisher Scientific, Waltham, MA, USA) using the ROX filter set in clear 96 well plates (Niesen *et al.*, 2007). The temperature was increased using a continuous ramp at a rate of 1°C/minute from 25°C to 95°C. Assays were performed in a final volume of 25 µl, containing 5 µM protein, 5X SYPRO Orange, 100 mM NaCl, 10 mM Na-HEPES, 1 mM MgCl<sub>2</sub>, 0.5 mM TCEP, pH 7.5, and different bisphosphonates concentrations (0.25-500 µM). Melting temperatures were extracted by Boltzmann sigmoidal fitting of the ascending phase of the curves.  $T_m$  dependence of the zoledronate concentration was fit using the Hill equation (Origin 7.0, OriginLab Corp., Northampton, MA, USA).

**Computational drug docking** – Coordinate files were prepared for molecular docking using the protein preparation wizard (Sastry *et al.*, 2013) (Schrödinger LLC, New York, NY). The protocol includes three stages: (1) addition of explicit hydrogens, bond order assignment and building missing amino acid sidechains; (2) determination of protonation state for protein sidechains using Propka 3.1 (Olsson *et al.*, 2011; Søndergaard *et al.*, 2011); (3) Restrained energy minimization with 0.3 RMSD cutoff for the heavy atoms. Ligprep (Schrödinger LLC, New York, NY) was used to prepare the known inhibitors of GGPPS for molecular docking. Ionization states of ligands were determined at pH of  $7.0 \pm 2.0$  using Epik 4.0 (Greenwood *et al.*, 2010). In addition to the normal protonation states, Epik generated metal binding states for each ligand. Molecular docking was performed using Glide 7.5 (Friesner *et al.*, 2004; Halgren *et al.*, 2004). The receptor grid was generated around the geometric center of the ligand found in the crystal structures, with 10Å edges for the enclosing box. Ligands were docked with flexible conformer sampling and the standard precision scoring function. The bisphosphonate core was restricted to the coordinates found in the crystal structure, with 0.5 Å tolerance for deviations. For each ligand up to ten different poses were generated, the pose with the lowest RMSD in comparison to the crystalized ligand was selected, and binding

## MOL # 117499

energy was estimated with mmGBSA (molecular mechanics - Generalized born and surface continuum solvation). The above method calculates binding energy using the equation:  $\Delta G_{\text{binding}} = G_{\text{complex}} - G_{\text{ligand}} - G_{\text{protein}}$ . The internal energy is calculated using the molecular mechanics OPLS3 forcefield (Harder *et al.*, 2016), while the desolvation energy and electrostatic interactions are calculated using VSGB (Variable Dielectric and Surface Generalized Born) (Li *et al.*, 2011). To account for the differences between Glide's scoring function and mmGBSA energies the ligand pose was optimized using energy minimization prior to the binding energy determination. Correlations between the calculated binding energies and the experimentally obtained values were calculated using the Pearson correlation coefficient.

MOL # 117499

## Results

**Crystal structure of hGGPPS in complex with bisphosphonate** – Bisphosphonates are used clinically in humans mainly for the treatment of osteoporosis (Russell, 2011). Although bisphosphonates are known to inhibit GGPPS, the structure of WT hGGPPS-bisphosphonate complex remained unresolved (Lisnyansky *et al.*, 2018). Importantly, the main molecular blueprint for designing novel bisphosphonate for GGPPS inhibition is the well characterized yGGPPS ortholog. Nevertheless, it was shown that bisphosphonates exhibit different affinities towards hGGPPS and yGGPPS, and their potency distributions differ for each enzyme (Guo *et al.*, 2007). Interestingly, in some cases the affinities differ by a factor of 20 between the enzymes, while in other cases, the affinities are practically identical. Therefore, in order to unveil the molecular details of hGGPPS-bisphosphonates interaction, we determined the 2.2 Å resolution crystal structure of hGGPPS in the presence of ibandronate (Figure 2, Supplemental Figure 1, Table 1, Data Supplement 1).

Similar to the previously reported structure of hGGPPS bound to GGPP (PDB 2Q80), the biological assembly consists of a hexamer, composed of a trimer of dimers (Figure 2A) (Kavanagh *et al.*, 2006a). Moreover, the structures share high similarity, as reflected by a low root mean square deviation (r.m.s.d.) value (0.63 Å) for the entire hexameric assembly, indicating that the binding of ibandronate does not induce major conformational transitions. Within the dimers, each monomer exhibits the canonical *trans*-prenyltransferase fold, composed of 13  $\alpha$ -helices. 10 of the 13  $\alpha$ -helices surround a large central cavity, where the aspartate-rich conserved sequence tandem, forming the FPP and bisphosphonate binding sites, is localized (Liang *et al.*, 2002).

Focusing on the bisphosphonate binding sites, we could identify three  $Mg^{2+}$  ions in five out of six chains and two  $Mg^{2+}$  ions in one chain (Figure 2B, Supplemental Figure 2). This is in contrast to the coordination of GGPP, which includes only two  $Mg^{2+}$  ions (Kavanagh *et al.*, 2006a). The  $Mg^{2+}$  ions in the hGGPPS-ibandronate structure are well coordinated, with an average  $Mg^{2+}$ -O bond length of  $2.19 \pm 0.21$  Å and a coordination number (CN) of  $5.7 \pm 0.6$  (range 4-6) for the entire hexamer. The Mg1 site is coordinated by two oxygens from the

MOL # 117499

phosphate group, two carboxyl oxygens from D64 and D68 and two water molecules (Figure 2C). The Mg<sub>2</sub> site is coordinated by one oxygen from the phosphate group, two carboxyl oxygens from D64 and D68 and three water molecules (Figure 2D). The Mg<sub>3</sub> site is coordinated by two oxygens from the phosphate group, one carboxyl oxygen from D188 and three water molecules (Figure 2E). Overall, each Mg<sup>2+</sup> ion is coordinated by 1-2 protein donor, 1-2 phosphate group donor and 2-3 water molecules, matching of the coordination observed in most Mg<sup>2+</sup>-protein complexes (Zheng *et al.*, 2008; Harding *et al.*, 2010). In summary, the first crystal structure of hGGPPS-bisphosphonate complex clearly supports the notion that three Mg<sup>2+</sup> ions are involved in the coordination of bisphosphonates by hGGPPS.

**Effect of Mg<sup>2+</sup> ions stoichiometry on drug docking to hGGPPS** – Next, we sought to assess the predictivity of our hGGPPS-ibandronate structure as a model for computational drug screening, and to determine the significance of Mg<sup>2+</sup> ions in hGGPPS-bisphosphonate interactions. To that end, we surveyed clinically available bisphosphonates and predicted their binding energies to the hGGPPS structure with Mg<sup>2+</sup> ions occupying all three sites (Table 2). To assess the contribution of Mg<sub>3</sub>, which was not resolved in one of the chains and is also absent in several yGGPPS structures (Guo *et al.*, 2007) (see below), we also performed this analysis with Mg<sup>2+</sup> ions occupying only sites Mg<sub>1</sub> and Mg<sub>2</sub> (Table 2). Next, we used our previously described thermal shift assay (TSA) to measure the binding affinities of six commercially available bisphosphonates to hGGPPS (Figure 3A, Supplemental Figure 3, Table 2) (Lisnyansky *et al.*, 2018). Strikingly, in the presence of all three Mg<sup>2+</sup> ions, the calculated binding energies are highly correlated with the measured K<sub>d</sub> values (R<sup>2</sup> = 0.93, p = 0.002, Figure 3B). In sharp contrast, removal of the Mg<sup>2+</sup> ion from the Mg<sub>3</sub> site resulted in deterioration of the models predictivity, resulting in poor correlation of the calculated binding energies with the K<sub>d</sub> (R<sup>2</sup> = 0.33, p = 0.23, Figure 3C).

Notably, the range of the measured K<sub>d</sub> values obtained for the commercially available compounds is rather narrow. Thus, we expanded our analysis by correlating previously reported pIC<sub>50</sub> values (Szabo *et al.*, 2002) spanning three orders of magnitude, with calculated binding energies in the presence of three or two Mg<sup>2+</sup> ions (Table 3, Figure 4A).

MOL # 117499

Again, a statistically significant correlation was obtained in the presence of all three  $Mg^{2+}$  ions between the calculated binding energies and the experimental  $IC_{50}$  values ( $R^2 = 0.62$ ,  $p < 0.0001$ , Figure 4A). Removal of the  $Mg^{2+}$  ion from the Mg3 site resulted in poor, non-significant, correlation of the calculated binding energies with the experimental  $IC_{50}$  values ( $R^2 = 0.14$ ,  $p = 0.075$ , Figure 4B). Thus, the structure of hGGPPS, solved in this study, is a highly useful model for computational drug docking studies. Moreover, the presence of  $Mg^{2+}$  ions in all three sites is imperative for ligand-protein interactions, and their assignment is a crucial prerequisite for successful docking.

**Re-analysis of yGGPPS-bisphosphonate complexes** – We have previously re-analyzed the structure of dimeric yGGPPS in complex with zoledronate (PDB 2E91) and were able to identify 3  $Mg^{2+}$  ions in each monomer (Lisnyansky *et al.*, 2018) with a coordination scheme similar to that reported here for hGGPPS in complex with ibandronate (Figure 2B, Figure 4A, Data Supplement 2). Importantly, two yGGPPS structures, in complex with BPH-252 (PDB 2Z4X, Data Supplement 3) and BPH-23 (PDB 2Z52, Data Supplement 4) were originally assigned with three  $Mg^{2+}$  ions per monomer. Thus, we decided to re-examine additional deposited structures of yGGPPS (Supplemental Table 1) with a goal of identifying previously unassigned  $Mg^{2+}$  ions. While the number of  $Mg^{2+}$  ions per monomer in the deposited structure varied between zero to three, we were able to assign three  $Mg^{2+}$  ions in all the re-refined structures (Table 4, Supplemental Figure 4). The structural validity of this analysis is supported by improvement in the crystallographic statistics, with significant decrease in  $R_{free}$ , markedly improved model stereochemistry and elimination of all the Ramachandran outliers in the deposited structures (Supplemental Table 1).

First, we analyzed deposited structures without any  $Mg^{2+}$  ions present. Given the surface electrostatics of the binding pocket (Figure 2B), encompassing the aspartate rich motifs, and of the phosphate groups, the absence of  $Mg^{2+}$  ions seemed highly unlikely. Indeed, while the original structures included no ions, we could position three  $Mg^{2+}$  ions in each chain (six ions in total) of yGGPPS-BPH806 (PDB 2Z78, Data Supplement 5) and yGGPPS-BPH-sc01 (PDB 2Z4Z, Data Supplement 6) (Supplemental Figure 4). In these cases, the average

MOL # 117499

Mg<sup>2+</sup>-O bond distance are  $2.40 \pm 0.25$  Å (yGGPPS-BPH-806) and  $2.23 \pm 0.25$  Å (yGGPPS-BPH-sc01), and in each structure five Mg<sup>2+</sup> ions have CN  $\geq 5$  and one ion has CN  $< 5$  (Table 4).

Next, we analyzed deposited structures with two Mg<sup>2+</sup> ions, similar to the case of yGGPPS-zoledronate (PDB 2E91). We have re-refined the structures of yGGPPS-minodronate (PDB 2E92, Data Supplement 7) and yGGPPS-BPH-675 (PDB 2E95, Data Supplement 8), with Mg<sup>2+</sup> ions assigned only at position Mg1 and Mg2, leaving the Mg3 site vacant. For yGGPPS-minodronate, following addition of Mg3 to both chains, the average Mg<sup>2+</sup>-O bond distance were  $2.17 \pm 0.13$  Å where three of the Mg<sup>2+</sup> ions have CN = 5 and three Mg<sup>2+</sup> ions have CN = 4 (Supplemental Figure 4, Table 4). Similarly, following addition of Mg3 to both chains of yGGPPS-BPH-675, the average Mg<sup>2+</sup>-O bond distance is  $2.14 \pm 0.12$  Å where all Mg<sup>2+</sup> ions have CN  $\geq 5$  (Supplemental Figure 4, Table 4).

Finally, we re-analyzed yGGPPS-BPH-210 (PDB 2Z7H, Data Supplement 9), where Mg<sup>2+</sup> binding differed between the chains: a single Mg<sup>2+</sup> ion was assigned to one monomer and no ions were assigned to the second monomer. As in the abovementioned structures, we could readily add five additional ions in total, with three Mg<sup>2+</sup> ions assigned to each chain (Supplemental Figure 4). The average Mg<sup>2+</sup>-O bond distance is  $2.24 \pm 0.23$  Å where all Mg<sup>2+</sup> ions have CN  $\geq 5$  (Table 4). Overall, we could identify three Mg<sup>2+</sup> ions per monomer in all of the re-refined structures presented here (Table 4), with an average CN =  $5.5 \pm 0.7$  (range = 3-6) and average Mg<sup>2+</sup>-O bond length =  $2.18 \pm 0.20$  Å, which closely match the expected values for Mg<sup>2+</sup> ions coordination (Table 4). Thus, re-refinement of these structures uncovers previously misidentified canonical binding scheme, demonstrating that similar to hGGPPS, bisphosphonates are binding to yGGPPS necessitates three Mg<sup>2+</sup> ions (Table 4, Supplemental Figure 4).

**Effect of Mg<sup>2+</sup> ions stoichiometry on drug docking to yGGPPS** – To further validate the assignment of Mg<sup>2+</sup> ions to the yGGPPS structures, and to generalize the functional significance of the metal-ligand stoichiometry, we performed additional virtual docking of

MOL # 117499

bisphosphonates with known  $K_i$  values towards  $\gamma$ GGPPS (PDB 2E91) (Figure 5B, Table 5) (Guo *et al.*, 2007). As in hGGPPS, to assess the contribution of Mg3, we performed this analysis with  $Mg^{2+}$  ions occupying all binding sites or only sites Mg1 and Mg2 (Table 5). Consistent with our crystallographic analysis (Figure 5A, Supplemental Figure 4), in the presence of all three  $Mg^{2+}$  ions, the calculated binding energies are highly correlated with the measured  $K_i$  values ( $R^2 = 0.71$ ,  $p = 0.0042$ , Figure 5B). However, leaving the Mg3 site vacant appreciably hindered the correlation between the calculated binding energies and the experimental  $K_i$  values ( $R^2 = 0.44$ ,  $p = 0.052$ , Figure 5C). Thus, a three  $Mg^{2+}$  ion stoichiometry is common and essential for binding of bisphosphonates to both  $\gamma$ GGPPS and hGGPPS.

MOL # 117499

## Discussion

The goals of the present study were to elucidate the structural basis of bisphosphonates with hGGPPS and to determine the accurate metal-ligand interactions network underlying GGPPS-bisphosphonates binding. In addition, given that mevalonate pathway enzymes, and specifically GGPPS, were highlighted in recent years as potential drug targets (Andela *et al.*, 2003; Jiang *et al.*, 2014; Gruenbacher and Thurnher, 2015), we sought to provide a reliable model for future drug design and screening. Importantly, preclinical studies have established the potential use of GGPPS inhibitors in the treatment of solid and hematological malignancies, such as lung alveolar carcinoma (Andela *et al.*, 2003) breast cancer (Ginestier *et al.*, 2012), multiple myeloma (Lacbay *et al.*, 2018), metastatic prostate cancer (Reilly *et al.*, 2015, 2017) and *KRAS*-mutant lung cancer (Xia *et al.*, 2014). Moreover, GGPPS enzymes from parasites leading to human diseases such as malaria, Chagas disease, leishmaniasis and toxoplasmosis are considered as potential drug targets as bisphosphonates were shown to inhibit parasitic growth *in vitro* and *in vivo* (Szabo *et al.*, 2002; Ricci *et al.*, 2016). Collectively, these data establish the clinical potential of GGPPS inhibitors.

Despite the promising preclinical results of GGPPS inhibitors, bisphosphonates have several shortcomings, currently preventing their clinical use in the treatment of non-skeletal diseases. Their main disadvantages relate to their pharmacokinetics, with limited distribution focused mainly to the bone matrix (Lin, 1996). In addition, some bisphosphonates lack specificity towards GGPPS (Guo *et al.*, 2007) and most of them display poor cell permeability (Haney *et al.*, 2017). Therefore, the design of novel bisphosphonates with improved tissue distribution profiles, such as the lipophilic bisphosphonates (Zhang *et al.*, 2009), bisphosphonates with improved GGPPS specificity (Zhou *et al.*, 2014; Wills *et al.*, 2015, 2017), and non-bisphosphonate GGPPS inhibitors is highly desired (Merino *et al.*, 2017). However, these translational efforts are hampered by the current ambiguity in metal-ligand interactions assignment within the binding site (Guo *et al.*, 2007; Hudock *et al.*, 2008; Zhang *et al.*, 2009), a problem common to other metalloenzymes as well (Puerta *et al.*, 2003). This ambiguity

MOL # 117499

impedes the ability of quantitative computational drug screening to predict protein-ligand interactions (Sommerhalter *et al.*, 2005; Riccardi *et al.*, 2018).

Although numerous yGGPPS structures in complex with different bisphosphonates are available, the affinity of these compounds towards hGGPPS and yGGPPS differs. For example, while the reported affinities of zoledronate and minodronate to yGGPPS are ~10 fold higher compared to hGGPPS, and the affinity of BPH-364 to yGGPPS is ~25 fold higher compared to hGGPPS, the affinity of other bisphosphonates such as BPH-628 and BPH-675 are practically identical for both orthologs (Guo *et al.*, 2007). Here, to provide a structural framework for the design of novel bisphosphonates for hGGPPS inhibition, we determined the first crystal structure of hGGPPS in complex with a bisphosphonate (Figure 2). Our 2.2 Å resolution crystal structure clearly resolved the hGGPPS-bisphosphonate bindings mode, involving three Mg<sup>2+</sup> ions. Rummaging through the protein data bank (PDB), we found this binding mode only in two yGGPPS-bisphosphonate complexes, but other metal stoichiometries ranging from zero to two Mg<sup>2+</sup> ions were reported in most structures (of which we have reanalyzed six and assigned the canonical three Mg<sup>2+</sup> ions) (Guo *et al.*, 2007; Hudock *et al.*, 2008; Zhang *et al.*, 2009). Thus, we sought to determine if the binding stoichiometry observed here for hGGPPS is a *bona fide* prerequisite for bisphosphonates binding, or if different bisphosphonates display different metal-ligand binding schemes.

While X-ray crystallography is the gold standard for high-resolution structural investigations, it should be kept in mind that the reported crystal structures are only models that explain the electron density, and are subjected to interpretation by the crystallographer (Davis *et al.*, 2003). The presence of metals, and specifically Mg<sup>2+</sup>, within ligand binding sites poses challenges in interpretation of the crystallographic data (Handing *et al.*, 2018). First, Mg<sup>2+</sup> has the same number of electrons as water, rendering them indistinguishable merely by their electron density. Thus, automatic assignment of water molecules to the model (Adams *et al.*, 2010), developed to facilitate structure determination, may become a double-edged sword by introducing bias and hampering the detection of other solvents such as Mg<sup>2+</sup>, Na<sup>+</sup> or NH<sub>4</sub><sup>+</sup> (Davis *et al.*, 2003), unless the added water molecules are critically examined. Moreover,

MOL # 117499

the wavelength required to detect  $Mg^{2+}$  by anomalous diffraction, an approach commonly used to identify other metals in metalloenzymes, is outside the wavelength range obtainable in modern synchrotrons (Zheng *et al.*, 2008, 2015; Harding *et al.*, 2010). Indeed, previous studies of structures deposited in the PDB revealed misidentification of  $Mg^{2+}$  ions in complex with RNA (Zheng *et al.*, 2015) or with metalloproteins (Zheng *et al.*, 2008), including placement of  $Mg^{2+}$  instead of  $Ca^{2+}$ ,  $Na^+$  or water and *vice versa*. The incorrect placement of  $Mg^{2+}$  within the binding pocket of metalloenzymes have clear implications on subsequent computational drug screening and design. As we show here, the omission of a single  $Mg^{2+}$  ion from the bisphosphonate binding scheme of either hGGPPS or yGGPPS results in poor model predictivity (Figure 3,4,5). These results emphasize the importance of metal-ligand interactions in computational drug screening and design in GGPPS and other metalloenzymes in general.

Of note, the calculated  $\Delta G$  values were positive, which indicates that the ligands would not bind, in stark conflict with reality. A close examination of the energy decomposition indicates that this is due to an overestimate of the electrostatic desolvation component of the binding free energy (Kessel and Ben-Tal, 2018), caused by the numerous charges on both the ligands and protein binding site. However, as all the molecules compared in this study share similar structure and as the protein structure changes very little when binding different bisphosphonates (Guo *et al.*, 2007), the error is subtracted out when comparing the relative values as observed in the slopes (Figures 3, 4, 5), even though the absolute  $\Delta G$  values are consistently too positive.

In light of the computational docking results, which decisively favored three  $Mg^{2+}$  ions in the bisphosphonate coordination scheme (Figure 3,4), we pursued a comprehensive re-analysis of previously deposited yGGPPS structures representing the four possible  $Mg^{2+}$  binding stoichiometries (Figure 5). Using a set of stereochemical restraints, including bond lengths, identity of oxygen donors and CN, we could place three  $Mg^{2+}$  ions in all the re-refined structures presented here (Table 4). Importantly, the overall bonding parameters were as expected based on the Cambridge structural database (CSD) and structures with similar

MOL # 117499

resolution deposited in the PDB (Zheng *et al.*, 2008). Together, our experimental and computational findings reiterate that Mg<sup>2+</sup> ions should be carefully placed in crystallographic structures based on the binding site geometry.

In conclusion, using the combination of experimental and computational approaches, we have established the metal coordination network mediating bisphosphonates-GGPPS interactions. Our data underscores the importance of three Mg<sup>2+</sup> ions in drug binding and their essential role in drug screening and design. This work provides a structural basis for future rational design of additional MBP-harboring drugs targeting hGGPPS.

MOL # 117499

**Supporting information.** Crystallographic statistics for the re-refined yGGPPS structures (Supplemental Table 1), crystal packing (Supplemental Figure 1), Mg<sup>2+</sup> ions omit map (Supplemental Figure 2), representative fluorescence-temperature relations of GGPPS in the presence of different ibandronate concentrations (Supplemental Figure 3), comparison of the deposited and re-refined yGGPPS binding pockets (Supplemental Figure 4). The structure of hGGPPS in complex with ibandronate and the re-refined yGGPPS structures are available as Data Supplements.

**Acknowledgements.** We thank the staff of ID30B at the ESRF for assistance with diffraction experimentation. This work was performed in partial fulfillment of the requirements for a Ph.D. degree of M.L. and a M.D. degree of O.S., Sackler Faculty of medicine, Tel Aviv University, Israel. We acknowledge the Edmund J. Safra Center for Bioinformatics at Tel-Aviv for supporting EY's PhD fellowship.

MOL # 117499

### **Authorship contribution**

Participated in research design: Giladi, Haitin.

Conducted experiments: Lisnyansky, Yariv, Segal, Marom.

Contributed new reagents or analytic tools: Loewenstein, Ben-Tal.

Performed data analysis: Lisnyansky, Giladi, Haitin.

Wrote or contributed to the writing of the manuscript: Lisnyansky, Giladi, Haitin.

**Conflict of interest statement.** The authors declare that no conflict of interest exists.

MOL # 117499

## References

- Adams PD, Afonine P V., Bunkóczi G, Chen VB, Davis IW, Echols N, Headd JJ, Hung LW, Kapral GJ, Grosse-Kunstleve RW, McCoy AJ, Moriarty NW, Oeffner R, Read RJ, Richardson DC, Richardson JS, Terwilliger TC, and Zwart PH (2010) PHENIX: A comprehensive Python-based system for macromolecular structure solution. *Acta Crystallogr Sect D Biol Crystallogr* **66**:213–221.
- Andela VB, Pirri M, Schwarz EM, Puzas EJ, O’Keefe RJ, Rosenblatt JD, and Rosier RN (2003) The Mevalonate Synthesis Pathway as a Therapeutic Target in Cancer. *Clin Orthop Relat Res* **415S**:S59-S66.
- Bourne HR, Sanders DA, and McCormick F (1990) The GTPase superfamily: A conserved switch for diverse cell functions. *Nature* **348**:125-132.
- Bruno E, Buemi MR, Di Fiore A, De Luca L, Ferro S, Angeli A, Cirilli R, Sadutto D, Alterio V, Monti SM, Supuran CT, De Simone G, and Gitto R (2017) Probing Molecular Interactions between Human Carbonic Anhydrases (hCAs) and a Novel Class of Benzenesulfonamides. *J Med Chem* **60**:4316–4326.
- Cohen SM (2017) A Bioinorganic Approach to Fragment-Based Drug Discovery Targeting Metalloenzymes. *Acc Chem Res* **50**:2007–2016.
- Davis AM, Teague SJ, and Kleywegt GJ (2003) Application and limitations of x-ray crystallographic data in structure-based ligand and drug design. *Angew Chem Int Ed Engl* **42**:2718-2736.
- Downward J (2003) Targeting RAS signalling pathways in cancer therapy. *Nat Rev Cancer* **3**:11–22.
- Emsley P, and Cowtan K (2004) Coot: Model-building tools for molecular graphics. *Acta Crystallogr Sect D Biol Crystallogr* **60**:2126–2132.
- Friesner RA, Banks JL, Murphy RB, Halgren TA, Klicic JJ, Mainz DT, Repasky MP, Knoll EH, Shelley M, Perry JK, Shaw DE, Francis P, and Shenkin PS (2004) Glide: a new approach for rapid, accurate docking and scoring. 1. Method and assessment of docking accuracy. *J Med Chem*, **47**:1739-1749.

MOL # 117499

Ginestier C, Monville F, Wicinski J, Cabaud O, Cervera N, Josselin E, Finetti P, Guille A, Larderet G, Viens P, Sebti S, Bertucci F, Birnbaum D, and Charafe-Jauffret E (2012) Mevalonate metabolism regulates basal breast cancer stem cells and is a potential therapeutic target. *Stem Cells* **30**:1327–1337.

Greenwood JR, Calkins D, Sullivan AP, and Shelley JC (2010) Towards the comprehensive, rapid, and accurate prediction of the favorable tautomeric states of drug-like molecules in aqueous solution. *J Comput Aided Mol Deg* **24**:591-604.

Gruenbacher G, and Thurnher M (2015) Mevalonate metabolism in cancer. *Cancer Lett* **356**:192-196.

Guo R-T, Cao R, Liang P-H, Ko T-P, Chang T-H, Hudock MP, Jeng W-Y, Chen CK-M, Zhang Y, Song Y, Kuo C-J, Yin F, Oldfield E, and Wang AH-J (2007) Bisphosphonates target multiple sites in both cis- and trans-prenyltransferases. *Proc Natl Acad Sci U S A* **104**:10022–10027.

Halgren TA, Murphy RB, Friesner RA, Beard HS, Frye LL, Pollard WT, and Banks JL (2004) Glide: A New Approach for Rapid, Accurate Docking and Scoring. 2. Enrichment Factors in Database Screening. *J Med Chem*, **47**:1750-1759.

Handing KB, Niedzialkowska E, Shabalina IG, Kuhn ML, Zheng H, and Minor W (2018) Characterizing metal-binding sites in proteins with X-ray crystallography. *Nat Protoc* **13**:1062–1090.

Haney SL, Wills VS, Wiemer DF, and Holstein SA (2017) Recent advances in the development of mammalian geranylgeranyl diphosphate synthase inhibitors. *Molecules* **22**:E886.

Harder E, Damm W, Maple J, Wu C, Reboul M, Xiang JY, Wang L, Lupyan D, Dahlgren MK, Knight JL, Kaus JW, Cerutti DS, Krilov G, Jorgensen WL, Abel R, and Friesner RA (2016) OPLS3: A Force Field Providing Broad Coverage of Drug-like Small Molecules and Proteins. *J Chem Theory Comput*, **12**:281-296.

Harding MM, Nowicki MW, and Walkinshaw MD (2010) Metals in protein structures: A review of their principal features. *Physiol Rev* **82**:331-371.

Hudock MP, Zhang Y, Guo R-T, Cao R, No JH, Liang P-H, Ko T-P, Chang T-H, Chang S,

MOL # 117499

- Song Y, Axelson J, Kumar A, Wang AH-J, and Oldfield E (2008) Inhibition of Geranylgeranyl Diphosphate Synthase by Bisphosphonates: A Crystallographic and Computational Investigation. *J Med Chem* **51**:5594–5607.
- Jiang P, Mukthavaram R, Chao Y, Nomura N, Bharati IS, Fogal V, Pastorino S, Teng D, Cong X, Pingle SC, Kapoor S, Shetty K, Aggrawal A, Vali S, Abbasi T, Chien S, and Kesari S (2014) In vitro and in vivo anticancer effects of mevalonate pathway modulation on human cancer cells. *Br J Cancer* **111**:1562–1571.
- Jiang Z, You Q, and Zhang X (2019) Medicinal chemistry of metal chelating fragments in metalloenzyme active sites: A perspective. *Eur J Med Chem* **165**:172-197.
- Kabsch W (2010) XDS. *Acta Crystallogr Sect D Biol Crystallogr* **66**:125–132.
- Kavanagh K. L., Dunford JE, Bunkoczi G, Russell RGG, and Oppermann U (2006a) The crystal structure of human geranylgeranyl pyrophosphate synthase reveals a novel hexameric arrangement and inhibitory product binding. *J Biol Chem* **281**:22004–22012.
- Kavanagh K. L., Guo K, Dunford JE, Wu X, Knapp S, Ebetino FH, Rogers MJ, Russell RGG, and Oppermann U (2006b) The molecular mechanism of nitrogen-containing bisphosphonates as antiosteoporosis drugs. *Proc Natl Acad Sci* **103**:7829–7834.
- Kennard O (2015) Cambridge Crystallographic Database. *Acta Crystallogr Sect A Found Crystallogr* **37**:C343–C343.
- Kessel A, and Ben-Tal N (2018) *Introduction to proteins: structure, function, and motions*, 2nd. ed. Taylor & Francis LLC., Boca Raton, FL.
- Konstantinopoulos PA, Karamouzis M V., and Papavassiliou AG (2007) Post-translational modifications and regulation of the RAS superfamily of GTPases as anticancer targets. *Nat Rev Drug Discov* **6**:541-555.
- Lacbay CM, Waller DD, Park J, Palou MG, Vincent F, Huang XF, Ta V, Berghuis AM, Sebag M, and Tsantrizos YS (2018) Unraveling the Prenylation-Cancer Paradox in Multiple Myeloma with Novel Geranylgeranyl Pyrophosphate Synthase (GGPPS) Inhibitors. *J Med Chem* **61**:6904–6917.
- Li J, Abel R, Zhu K, Cao Y, Zhao S, and Friesner RA (2011) The VSGB 2.0 model: A next

MOL # 117499

- generation energy model for high resolution protein structure modeling. *Proteins* **79**:2794-2812.
- Liang PH, Ko TP, and Wang Andrew H J (2002) Structure, mechanism and function of prenyltransferases. *Eur J Biochem* **269**:3339-3354.
- Lin JH (1996) Bisphosphonates: A review of their pharmacokinetic properties. *Bone* **18**:75-85.
- Lisnyansky M, Kapelushnik N, Ben-Bassat A, Marom M, Loewenstein A, Khananshvili D, Giladi M, and Haitin Y (2018) Reduced Activity of Geranylgeranyl Diphosphate Synthase Mutant Is Involved in Bisphosphonate-Induced Atypical Fractures. *Mol Pharmacol* **94**:1391–1400.
- McCoy AJ, Grosse-Kunstleve RW, Adams PD, Winn MD, Storoni LC, and Read RJ (2007) Phaser crystallographic software. *J Appl Crystallogr* **40**:658–674.
- Merino P, Maiuolo L, Delso I, Algieri V, De Nino A, and Tejero T (2017) Chemical approaches to inhibitors of isoprenoid biosynthesis: targeting farnesyl and geranylgeranyl pyrophosphate synthases. *RSC Adv* **7**:10947-10967.
- Mullen PJ, Yu R, Longo J, Archer MC, and Penn LZ (2016) The interplay between cell signalling and the mevalonate pathway in cancer. *Nat Rev Cancer* **16**:718-731.
- Nayal M, and Di Cera E (1996) Valence screening of water in protein crystals reveals potential Na<sup>+</sup> binding sites. *J Mol Biol* **256**:228–234.
- Niesen FH, Berglund H, and Vedadi M (2007) The use of differential scanning fluorimetry to detect ligand interactions that promote protein stability. *Nat Protoc* **2**:2212–2221.
- Olsson MHM, SØndergaard CR, Rostkowski M, and Jensen JH (2011) PROPKA3: Consistent treatment of internal and surface residues in empirical p K a predictions. *J Chem Theory Comput* **7**:525-537.
- Puerta DT, Schames JR, Henchman RH, McCammon JA, and Cohen SM (2003) From model complexes to metalloprotein inhibition: A synergistic approach to structure-based drug discovery. *Angew Chemie - Int Ed* **42**:3772–3774.
- Reilly JE, Neighbors JD, and Hohl RJ (2017) Targeting protein geranylgeranylation slows tumor development in a murine model of prostate cancer metastasis. *Cancer Biol Ther*

MOL # 117499

18:872–882.

Reilly JE, Neighbors JD, Tong H, Henry MD, and Hohl RJ (2015) Targeting geranylgeranylation reduces adrenal gland tumor burden in a murine model of prostate cancer metastasis. *Clin Exp Metastasis* **32**:555–566.

Riccardi L, Genna V, and De Vivo M (2018) Metal–ligand interactions in drug design. *Nat Rev Chem* **2**:100–112.

Ricci CG, Liu YL, Zhang Y, Wang Y, Zhu W, Oldfield E, and McCammon JA (2016) Dynamic Structure and Inhibition of a Malaria Drug Target: Geranylgeranyl Diphosphate Synthase. *Biochemistry* **55**:5180–5190.

Russell RGG (2011) Bisphosphonates: The first 40 years. *Bone* **49**:2-19.

Sastry GM, Adzhigirey M, Day T, Annabhimoju R, and Sherman W (2013) Protein and ligand preparation: Parameters, protocols, and influence on virtual screening enrichments. *J Comput Aided Mol Des* **27**:221-234.

Sommerhalter M, Lieberman RL, and Rosenzweig AC (2005) X-ray crystallography and biological metal centers: Is seeing believing? *Inorg Chem* **44**:770-778.

Søndergaard CR, Olsson MHM, Rostkowski M, and Jensen JH (2011) Improved treatment of ligands and coupling effects in empirical calculation and rationalization of p K<sub>a</sub> values. *J Chem Theory Comput* **7**:2284-2295.

Strong M, Sawaya MR, Wang S, Phillips M, Cascio D, and Eisenberg D (2006) Toward the structural genomics of complexes: crystal structure of a PE/PPE protein complex from *Mycobacterium tuberculosis*. *Proc Natl Acad Sci U S A* **103**:8060–8065.

Szabo CM, Matsumura Y, Fukura S, Martin MB, Sanders JM, Sengupta S, Cieslak JA, Loftus TC, Lea CR, Lee HJ, Koohang A, Coates RM, Sagami H, and Oldfield E (2002) Inhibition of geranylgeranyl diphosphate synthase by bisphosphonates and diphosphates: A potential route to new bone antiresorption and antiparasitic agents. *J Med Chem* **45**:2185–2196.

Wang M, and Casey PJ (2016) Protein prenylation: Unique fats make their mark on biology.

Wills VS, Allen C, Holstein SA, and Wiemer DF (2015) Potent Triazole Bisphosphonate

MOL # 117499

Inhibitor of Geranylgeranyl Diphosphate Synthase. *ACS Med Chem Lett* **6**:1195–1198.

Wills VS, Metzger JI, Allen C, Varney ML, Wiemer DF, and Holstein SA (2017)

Bishomoisoprenoid triazole bisphosphonates as inhibitors of geranylgeranyl diphosphate synthase. *Bioorganic Med Chem* **25**:2437–2444.

Xia Y, Liu YL, Xie Y, Zhu W, Guerra F, Shen S, Yeddula N, Fischer W, Low W, Zhou X, Zhang

Y, Oldfield E, and Verma IM (2014) A combination therapy for kras-Driven lung adenocarcinomas using lipophilic bisphosphonates and rapamycin. *Sci Transl Med* **6**:263ra161.

Zhang Y, Cao R, Yin F, Hudock MP, Guo RT, Krysiak K, Mukherjee S, Gao YG, Robinson H,

Song Y, No JH, Bergan K, Leon A, Cass L, Goddard A, Chang TK, Lin FY, Beek E Van, Papapoulos S, Wang AHJ, Kubo T, Ochi M, Mukkamala D, and Oldfield E (2009) Lipophilic bisphosphonates as dual farnesyl/geranylgeranyl diphosphate synthase inhibitors: An X-ray and nmr investigation. *J Am Chem Soc* **131**:5153–5162.

Zheng H, Chruszcz M, Lasota P, Lebioda L, and Minor W (2008) Data mining of metal ion

environments present in protein structures. *J Inorg Biochem* **102**:1765–1776.

Zheng H, Shabalin IG, Handing KB, Bujnicki JM, and Minor W (2015) Magnesium-binding

architectures in RNA crystal structures: Validation, binding preferences, classification and motif detection. *Nucleic Acids Res* **43**:3789–3801.

Zhou X, Ferree SD, Wills VS, Born EJ, Tong H, Wiemer DF, and Holstein SA (2014) Geranyl

and neryl triazole bisphosphonates as inhibitors of geranylgeranyl diphosphate synthase. *Bioorganic Med Chem* **22**:2791–2798.

MOL # 117499

### **Footnotes**

This work was supported by Israel Science Foundation [grant numbers 1721/16, 1775/12] (Y.H.), Israel Cancer Research Foundation [grant number 01214] (Y.H.), German-Israeli Foundation [grant number I-2425-418.13/2016] (Y.H.), the Shtacher foundation (Y.H. and M.G.) and Tel-Aviv Sourasky Medical Center (A.L. and M.G.).

MOL # 117499

## Figure legends

**Figure 1. Catalytic cycle of GGPPS.** FPP (C<sub>15</sub>) and IPP (C<sub>5</sub>) are condensed by GGPPS to form GGPP (C<sub>20</sub>). The geranylgeranyl moiety is then transferred from GGPP to a C-terminal CAAX motif (C-cysteine, A-aliphatic residue, X-Leucine/Phenylalanine) by GGPTase (geranylgeranyl protein transferase), resulting in membrane association of small GTPases.

**Figure 2. Crystal structure of hGGPPS in complex with ibandronate.** (A) The asymmetric unit, containing the biological hexameric arrangement of ibandronate-bound hGGPPS, in cartoon representation. (B) Surface representation of one monomer colored according to the adaptive Poisson-Boltzmann solver surface electrostatics. The rectangle frames a zoom perspective of the ibandronate binding pocket. Ibandronate and residues interacting with the Mg<sup>2+</sup> ions (purple spheres) are shown as sticks. Water molecules are shown as red spheres. (C, D, E) The three Mg<sup>2+</sup> binding sites, Mg1 (C), Mg2 (D) and Mg3 (E) are shown with their electron density contoured at 1.3σ (blue mesh).

**Figure 3. Effect of Mg<sup>2+</sup> stoichiometry on computational docking of commercial bisphosphonates to hGGPPS.** (A) Differential scanning fluorimetry thermal shift assay in the presence of increasing bisphosphonates concentrations presented as *T<sub>m</sub>* difference. Experiments were performed as outlined in Materials and Methods. Data are presented as mean ± SD, n = 6. (B,C) Correlation between measured K<sub>d</sub> values (μM) and calculated binding energies (Kcal/mol) obtained with Mg<sup>2+</sup> ions occupying all three Mg<sup>2+</sup> sites (B) or only sites Mg1 and Mg2 (C).

**Figure 4. Extended analysis of Mg<sup>2+</sup> effect on computational docking of bisphosphonates to hGGPPS.** (A,B) Correlation between measured IC<sub>50</sub> values (μM) (reported by Szabo et al., 2002) and calculated binding energies (Kcal/mol) obtained with Mg<sup>2+</sup> ions occupying all three Mg<sup>2+</sup> sites (A) or only sites Mg1 and Mg2 (B).

**Figure 5. Effect of Mg<sup>2+</sup> stoichiometry on computational docking of bisphosphonates to yGGPPS.** (A) Cartoon representations of the ligand binding pocket in the deposited zoledronate-bound yGGPPS (PDB 2E91, upper panel) and the re-refined structure (lower

MOL # 117499

panel). Zoledronate and residues interacting with the  $Mg^{2+}$  ions (purple spheres) are shown as sticks. Water molecules are shown as red spheres. **(B,C)** Correlation between reported  $K_i$  values (nM) and calculated binding energies (Kcal/mol) obtained with  $Mg^{2+}$  ions occupying all three  $Mg^{2+}$  sites (B) or only sites Mg1 and Mg2 (C).

MOL # 117499

**Table 1. Crystallographic statistics for hGGPPS in complex with ibandronate**

<b>Data collection</b>	
<b>Spacegroup</b>	P2 <sub>1</sub> 2 <sub>1</sub> 2 <sub>1</sub>
<b>Cell dimensions</b>	
<b>a,b,c (Å)</b>	68.40, 152.80, 198.40
<b>α,β,γ (°)</b>	90, 90, 90
<b>Beamline</b>	ESRF ID30B
<b>Wavelength (Å)</b>	0.976
<b>Resolution (Å)</b>	2.2
<b>Multiplicity</b>	6.58
<b>Completeness (%)</b>	99.8
<b>Mean I/σ(I)</b>	8.51
<b>R<sub>meas</sub> (%)</b>	17.1
<b>Refinement statistics</b>	
<b>No. reflections (work/free)<sup>a</sup></b>	98591/5215
<b>Resolution range<sup>a</sup></b>	49.66-2.20
<b>R<sub>work</sub>/R<sub>free</sub></b>	0.1787/0.2245
<b>No. atoms</b>	
<b>Macromolecules</b>	13678
<b>Ligands</b>	143
<b>Solvent</b>	1242
<b>Average B-factor</b>	
<b>Macromolecules</b>	36.3
<b>Ligands</b>	51.0
<b>Solvent</b>	43.0
<b>RMSD (bond lengths)</b>	0.005
<b>RMSD (bond angles)</b>	0.8
<b>Ramachandran outliers (%)</b>	0

ESRF, European Synchrotron Radiation Facility; RMSD, root-mean-square deviation.

<sup>a</sup> after anisotropic scaling

MOL # 117499

**Table 2. Experimental and calculated binding parameters of bisphosphonates to hGGPPS.**

Bisphosphonate	$\Delta T_m$	$K_d$ ( $\mu\text{M}$ )	calculated $\Delta G$ (Kcal/mol)	
			3 $\text{Mg}^{2+}$	2 $\text{Mg}^{2+}$
Ibandronate	$23.9 \pm 0.6$	$1.74 \pm 0.22$	21.1	22.1
Zoledronate	$19.6 \pm 0.4$	$2.76 \pm 0.31$	25.3	30.8
Alendronate	$16.0 \pm 0.2$	$3.03 \pm 0.21$	30.3	36.2
Risedronate	$16.8 \pm 0.3$	$3.35 \pm 0.30$	30.6	48.4
Neridronate	$17.4 \pm 0.3$	$3.51 \pm 0.30$	32.1	31.5
Pamidronate	$15.8 \pm 0.3$	$4.40 \pm 0.45$	34.1	33.3

$T_m$ , melting temperature;  $\Delta G$  values were calculated as described in materials and methods.

The average  $\Delta T_m$  and  $K_d$  values are shown as average  $\pm$  SD,  $n = 6$  for all the experiments.

MOL # 117499

**Table 3. Experimental IC<sub>50</sub> values and calculated binding energies of bisphosphonates to hGGPPS.**

Bisphosphonate	IC <sub>50</sub> (μM)	calculated ΔG (Kcal/mol)	
		3 Mg <sup>2+</sup>	2 Mg <sup>2+</sup>
14	0.92	0.22	31.63
15	1.4	0.02	22.84
16	0.72	8.92	41.94
17	4.3	21.05	30.49
18	11	18.44	36.45
19	53	16.74	34.55
20	200	17.32	34.07
21	620	20.09	38.45
22	180	28.76	44.18
23	220	25.19	42.65
24	220	22.48	39.44
25	220	28.58	31.15
26	260	31.05	28.52
27	350	22.63	42.69
28	410	30.93	40.82
29	550	27.78	37.25
30	2.2	10.04	20.47
31	19	6.77	8.52
32	83	10.64	21.01
33	330	24.42	32.05
34	690	19.87	36.01
35	440	23.72	33.29
36	180	27.95	45.70

IC<sub>50</sub> were obtained from Szabo et al., 2002. For full description of the compounds, please refer to the original publication. ΔG values were calculated as described in materials and methods.

MOL # 117499

**Table 4. Mg<sup>2+</sup> coordination parameters in re-refined structures of yGGPPS.**

Ligand	PDB	Mg <sup>2+</sup> /chain (deposited)	Mg <sup>2+</sup> /chain (re- refined)	Mg <sup>2+</sup> -O bond length (Å)	CN ≥ 5	CN < 5
Zoledronate	2E91	2	3	2.09 ± 0.13 (34)	6	0
Minodronate	2E92	2	3	2.17 ± 0.13 (27)	3	3
BPH-675	2E95	2	3	2.14 ± 0.12 (35)	6	0
BPH-210	2Z7H	0/1	3	2.24 ± 0.23 (33)	6	0
BPH-806	2Z78	0	3	2.40 ± 0.25 (31)	5	1
BPH-sc01	2Z4Z	0	3	2.23 ± 0.25 (31)	5	1
BPH-252	2Z4X	3	3	2.11 ± 0.10 (36)	6	0
BPH-23	2Z52	3	3	2.10 ± 0.17 (36)	6	0

CN, coordination number. The average Mg<sup>2+</sup>-O bond length is shown as average ± SD, numbers in parentheses indicate the sample size.

MOL # 117499

**Table 5. Experimental and calculated binding parameters of bisphosphonates to  $\gamma$ GGPPS.**

Bisphosphonate	Experimental $K_i$ (nM)	calculated $\Delta G$ (Kcal/mol)	
		3 $Mg^{2+}$	2 $Mg^{2+}$
BPH-364	10	21.1	14.4
BPH-628	30	27.5	27.5
BPH-676	30	24.9	19.1
BPH-608	60	39.1	33.3
BPH-675	80	31.4	26.4
BPH-629	110	51.0	44.4
BPH-210	115	30.7	14.5
Minodronate	130	45.3	29.0
Zoledronate	260	57.9	51.4

$K_i$  values were obtained from Guo et al., 2007. For full description of the compounds, please refer to the original publication.  $\Delta G$  values were calculated as described in materials and methods.

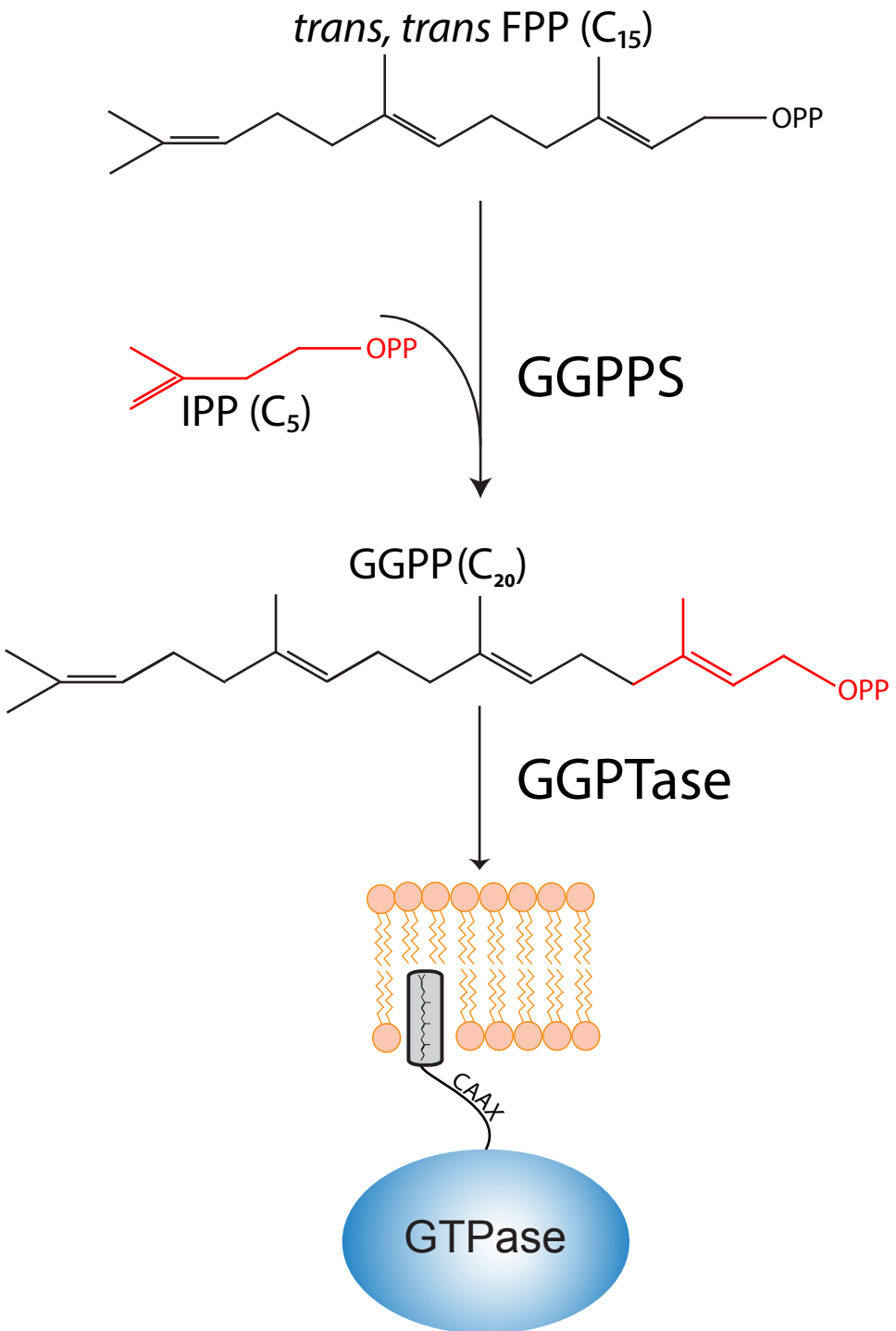


Figure 1

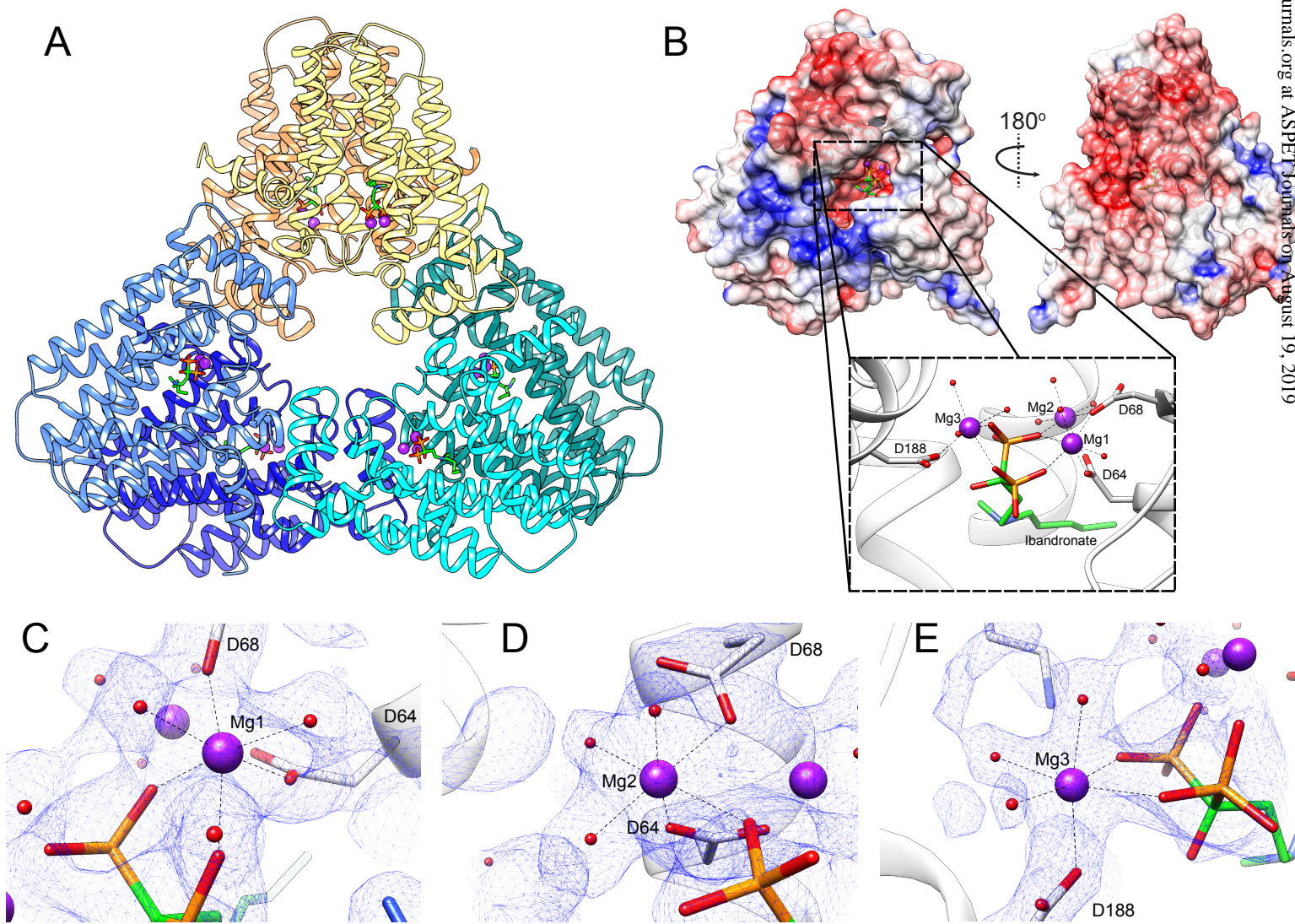


Figure 2

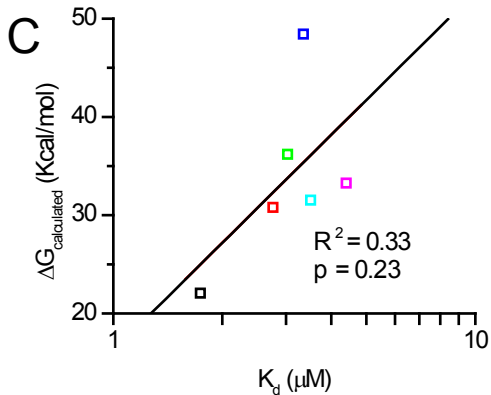
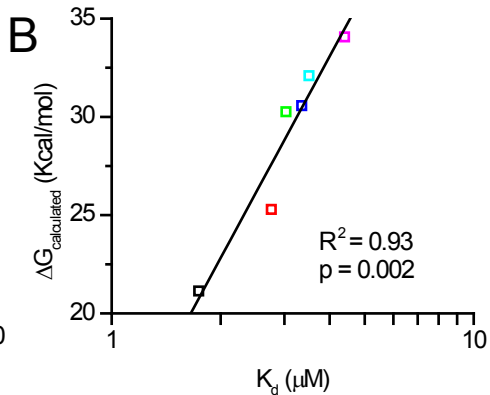
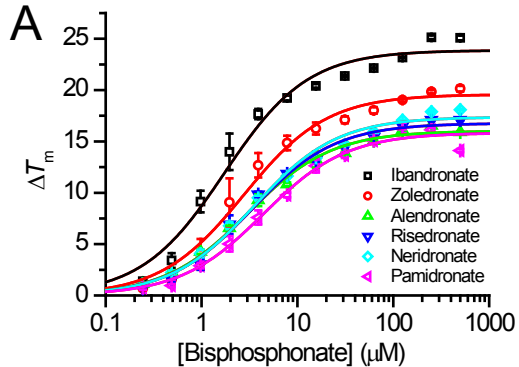


Figure 3

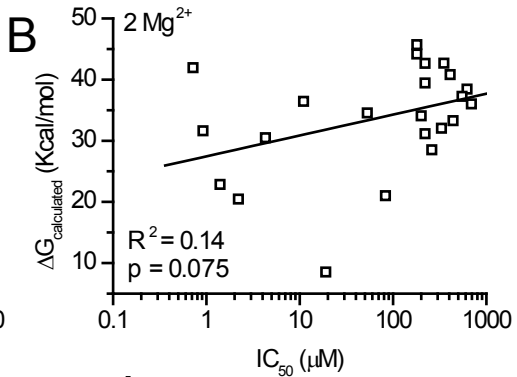
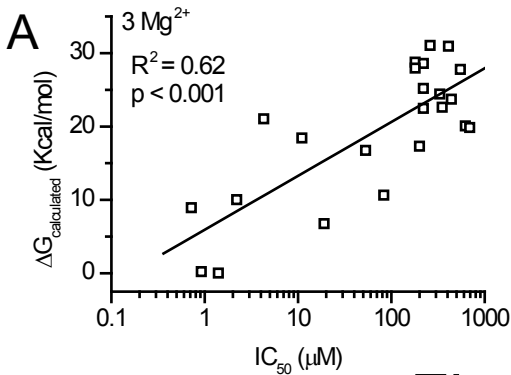
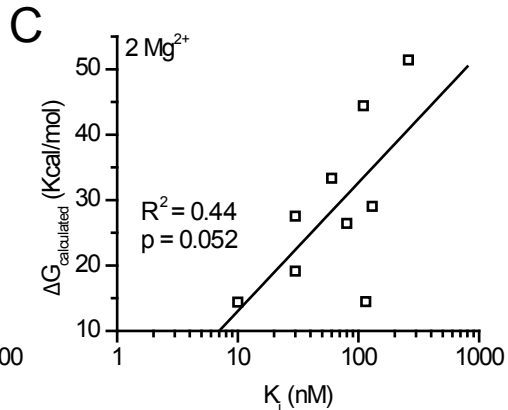
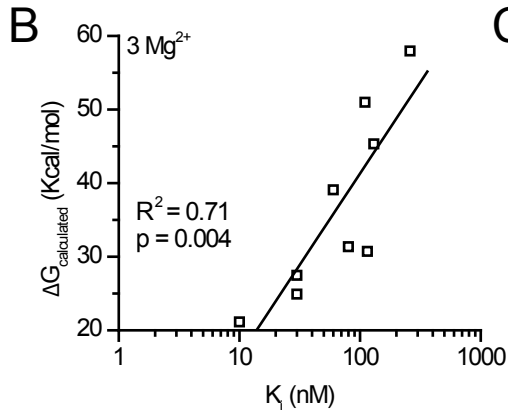
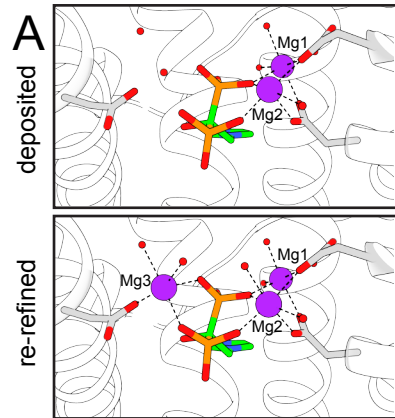


Figure 4



**Figure 5**